Title: Porcine deltacoronavirus induces caspase-dependent apoptosis through activation of the cytochrome *c*-mediated intrinsic mitochondrial pathway

Authors: Yoo Jin Lee, Changhee Lee

PII: S0168-1702(18)30226-0
DOI: https://doi.org/10.1016/j.virusres.2018.06.008
Reference: VIRUS 97428

To appear in: *Virus Research*

Received date: 16-4-2018
Revised date: 9-6-2018
Accepted date: 20-6-2018

Please cite this article as: Lee YJ, Lee C, Porcine deltacoronavirus induces caspase-dependent apoptosis through activation of the cytochrome *c*-mediated intrinsic mitochondrial pathway, *Virus Research* (2018), https://doi.org/10.1016/j.virusres.2018.06.008

Porcine deltacoronavirus induces caspase-dependent apoptosis through activation of the cytochrome *c*-mediated intrinsic mitochondrial pathway

Yoo Jin Lee and Changhee Lee*

Animal Virology Laboratory, School of Life Sciences, BK21 Plus KNU Creative BioResearch Group, Kyungpook National University, Daegu 41566, Republic of Korea

* Corresponding author mailing address:
School of Life Sciences
College of Natural Sciences
Kyungpook National University
Daegu 41566
Republic of Korea
Phone: +82-53-950-7365
Fax: +82-53-955-5522
Email: changhee@knu.ac.kr

Highlights

- Caspase-9 and caspase-3 activation was involved in the replication of PDCoV.
- PDCoV infection stimulated MOMP either via Bax recruitment or MPTP opening.
- PDCoV-mediated MOMP resulted in apoptogenic cytochrome *c* release into the cytoplasm.
- Mitochondrial cytochrome *c* leakage executed apoptotic cell death in PDCoV infection.
- Caspase-dependent intrinsic apoptosis beneficially contributes to PDCoV replication.

ABSTRACT

Porcine deltacoronavirus (PDCoV), a newly discovered enteric coronavirus, is a causative agent of severe clinical diarrhea and intestinal pathological damage in piglets. As a first step toward understanding the effect of PDCoV on host cells, we elucidated mechanisms underlying the process of apoptotic cell death after PDCoV infection. The use of a pan-caspase inhibitor resulted in the inhibition of PDCoV-induced apoptosis and reduction of PDCoV replication, suggestive of the association of a caspase-dependent pathway. Furthermore, PDCoV infection necessitated the activation of the initiator caspase-9 responsible for the intrinsic mitochondrial apoptosis pathway. Experimental data indicated that PDCoV infection led to Bax-mediated mitochondrial outer membrane permeabilization (MOMP), resulting in specific relocation of the mitochondrial cytochrome *c* (cyt c) into the cytoplasm. Treatment with cyclosporin A (CsA), an inhibitor of mitochondrial permeability transition pore (MPTP) opening, significantly suppressed PDCoV-triggered apoptosis and viral replication. Moreover, cyt c release was completely abrogated in PDCoV-infected cells in the presence of CsA, suggesting the critical role of MPTP in intrinsic apoptosis in response to PDCoV infection. Altogether, our results indicate that PDCoV infection stimulates MOMP either via Bax recruitment or MPTP opening to permit the release of apoptogenic cyt c into the cytoplasm, thereby leading to execution of the caspase-dependent intrinsic apoptosis pathway to facilitate viral replication *in vitro*.

Keywords: PDCoV; Apoptotic cell death; MOMP; Cytochrome c; Caspase-dependent intrinsic pathway

1. Introduction

Porcine deltacoronavirus (PDCoV), a member of the genus *Deltacoronavirus* in the family *Coronaviridae* of the order *Nidovirales*, is a novel emerging pathogenic enterocyte-tropic swine coronavirus (Jung et al., 2015; Woo et al., 2012). PDCoV infection is marked by acute, watery diarrhea and vomiting, ultimately leading to dehydration and mortality in suckling piglets (Jung et al., 2015; Ma et al., 2015). Since its first discovery in Hong Kong in 2012 (Woo et al., 2012), this virus has emerged globally, especially in the North American and Asian pig-producing countries (Lee and Lee, 2014; Madapong et al., 2016; Saeng-Chuto et al., 2017; Song et al., 2015; Wang et al., 2015; Woo et al., 2012; Li et al., 2014; Marthaler et al., 2014).

PDCoV is transmitted via the fecal-oral route and replicates in the cytoplasm of the villous epithelial cells throughout the small intestine (Chen et al., 2015; Jang et al., 2018; Jung et al., 2015). Infected small intestinal enterocytes undergo vacuolation and extensive exfoliation of the villous epithelium, followed by villous atrophy (Chen et al., 2015; Jang et al., 2018; Jung et al., 2015). The massive loss of enterocytes hampers the absorption and digestion of nutrients and electrolytes in the small intestine, thereby causing malabsorptive and maldigestive diarrhea and the consequent fatal dehydration in piglets (Jung et al., 2015). The pathophysiological change, including vacuolar degeneration and eventual death of enterocytes, is likely associated with necrosis caused by the cytolytic action of the virus, as PDCoV fails to induce apoptosis in infected intestinal enterocytes *in vivo* (Jung et al., 2016).

PDCoV can be propagated in swine-origin epithelial cell lines, LLC porcine kidney (LLC-PK) and swine testicle (ST) cells (Hu et al., 2015). Cytopathic effects (CPE) of PDCoV in both cell lines are comparable and consist of enlarged, rounded, and granular cells that undergo cell shrinkage and detachment (Hu et al., 2015; Jang et al., 2018). In contrast to *in vivo* circumstances,

the cytopathological alteration in PDCoV-infected LLC-PK and ST cells are known to occur via apoptosis and directly related to the viral replication *in vitro* (Jung et al., 2016). However, the molecular mechanisms that induce apoptosis in PDCoV-infected cell lines remain poorly understood. Therefore, in this study, we aimed to define the specific pathways involved in the apoptotic death of PDCoV-infected ST cells *in vitro*.

2. Material and methods

2.1. Cells, virus, reagents, and antibodies

ST cells were cultured in alpha minimum essential medium (α-MEM; Invitrogen, Carlsbad, CA) with 5% fetal bovine serum (FBS; Invitrogen) and antibiotic-antimycotic solutions (100×; Invitrogen). The cells were maintained at 37 °C in a humidified 5% CO_2 incubator. PDCoV strain KNU16-07 was propagated in ST cells in virus growth medium [α-MEM supplemented with antibiotic-antimycotic solutions, 10 mM HEPES (Invitrogen), and 5 μg/ml of trypsin] without FBS as described previously (Jang et al, 2018). Mock-infected ST cells were also maintained under the same condition with virus growth medium in the absence of FBS. Staurosporine was obtained from Cayman Chemical Company (Ann Arbor, MI) and used at a concentration of 1 μg/ml to induce apoptosis. Pan-caspase inhibitor (Z-VAD-FMK), caspase-8 inhibitor (Z-IETD-FMK), and caspase-9 inhibitor (Z-LEHD-FMK) were purchased from R&D systems (Minneapolis, MN). Cyclosporin A (CsA) and *N*-phenylmaleimide (*N*-PhMI) were obtained from Cell Signaling Technologies (Danvers, MA) and Sigma-Aldrich (St. Louis, MO), respectively. All reagents were dissolved in dimethyl sulfoxide (DMSO) and present during the entire period of virus infection or mock infection. The PDCoV nucleocapsid (N) protein-specific monoclonal antibody (MAb) was described previously (Jang et al., 2018). Antibodies specific for cytochrome *c* (cyt c), apoptosis-

inducing factor (AIF), Bax, Sp1, and β-actin and horseradish peroxidase (HRP)-conjugated secondary antibodies were obtained from Santa Cruz Biotechnology (Santa Cruz, CA). The caspase-3, caspase-9, voltage-dependent anion channel (VDAC), and α-tubulin antibodies were purchased from Sigma-Aldrich.

2.2. Cell viability assay

The cytotoxic effects of reagents on ST cells were analyzed using a colorimetric 3-(4,5-dimethylthiazol-2-yl)-2,5-diphenyltetrazolium bromide (MTT) assay (Sigma-Aldrich) to detect cell viability. Briefly, ST cells were grown at 1×10^4 cells/well in a 96-well tissue culture plate and treated with each chemical for 24 h. After 1 day of incubation, 50 μl of MTT solution (1.1mg/ml) was added to each well, and the samples were incubated for an additional 4 h. The supernatant was then removed from each well, after which 150 μl of DMSO was added to dissolve the colored formazan crystals produced by the MTT. The absorbance of the solution was measured at 540 nm using an enzyme-linked immunosorbent assay plate reader. All MTT assays were performed in triplicate.

2.3. DNA fragmentation assay

ST cells were grown at 3.5×10^5 cells/well in 6-well tissue culture plates for 1 day and then mock infected or infected with PDCoV at a multiplicity of infection (MOI) of 1. In addition, cells were pretreated with Z-VAD-FMK or CsA for 1 h followed by PDCoV infection. At the indicated times, cells were harvested, washed with PBS, and then incubated in a cell lysis buffer (10 mM Tris, pH 7.5, 1 mM EDTA, and 0.2% Triton X-100) containing 500 μg/ml protease K for 24 h at 55 °C. The DNA was then extracted twice with phenol/chloroform, precipitated with

isopropanol, and resuspended in distilled water. Next, the purified DNA was incubated with 20 μg/ml ribonuclease A for 1 h at 37 °C, electrophoresed on a 1.2% agarose gel containing Midori Green Advanced DNA Stain (NIPPON Genetics, Tokyo, Japan), and photographed.

2.4. TUNEL labeling assay

ST cells were grown on microscope coverslips placed in 6-well tissue culture plates and mock infected or infected with PDCoV at a MOI of 1. The virus-infected cells were fixed at 12 hours post-infection (hpi) with 4% paraformaldehyde for 25 min at 4 °C and permeabilized with 0.2% Triton X-100 in PBS at RT for 5 min. A terminal deoxynucleotidyl transferase-catalyzed deoxyuridine phosphate-nick end labeling (TUNEL) assay was performed using a DeadEnd Fluorometric TUNEL System kit (Promega, Madison, WI) according to the manufacturer's instructions with some modifications. Briefly, PDCoV-infected ST cells were rinsed twice with PBS, and the TUNEL reaction mixture was added, incubated for 60 min at 37°C, immersed in 2×SSC buffer for 15 min, and washed 3 times in PBS. TUNEL-labeled cells were subjected to immunofluorescence using N-specific MAb and Alexa Fluor 594-conjugated goat anti-mouse antibody as described below. The samples were mounted on microscope glass slides in mounting buffer (60% glycerol and 0.1% sodium azide in PBS) and analyzed under a Confocal Laser Scanning microscope (Carl Zeiss, Gattingen, Germany) using an excitation wavelength in the range of 450–500 nm and an emission wavelength in the range of 515–565 nm.

2.5. Annexin V and PI staining assay

ST cells were grown in 6-well tissue culture plates for 1 day and mock infected or infected with PDCoV at an MOI of 1. To examine the effect of each inhibitor on PDCoV-induced apoptosis,

cells were treated with Z-VAD-FMK or CsA and then infected with PDCoV. The virus-inoculated cells were further propagated in the presence of Z-VAD-FMK (100 μM), CsA (10 μM) or DMSO (0.5%; vehicle control). Phosphatidylserine exposure was determined by measuring Annexin V binding at the indicated times using an Alexa Fluor 488 Annexin V/Dead Cell Apoptosis kit (Invitrogen), according to the manufacturer's protocol. In brief, cells were harvested, washed with cold PBS, and suspended in 100 μl 1× annexin-binding buffer. The cells were then incubated with Alexa Fluor 488-conjugated Annexin V and propidium iodide (PI) at room temperature (RT) for 15 min in the dark. Following the incubation period, 400 μl of annexin-binding buffer was added to each sample, and the samples were mixed gently and kept on ice. The fluorescent signals of Annexin V and PI were detected at channels FL-1 and FL-2, respectively, and analyzed using a fluorescence-activated cell sorter (FACS) Aria III flow cytometer (BD Biosciences, San Jose, CA). Cells negative for PI uptake and positive for Annexin V were considered apoptotic.

2.6. Immunofluorescence assay (IFA)

ST cells grown on microscope coverslips placed in 6-well tissue culture plates were pretreated with each reagent or DMSO for 1 h and mock infected or infected with PDCoV at a MOI of 1. The virus-infected cells were subsequently grown in the presence of inhibitors until 12 hpi, fixed with 4% paraformaldehyde for 10 min at RT and permeabilized with 0.2% Triton X-100 in PBS at RT for 10 min. The cells were blocked with 1% bovine serum albumin (BSA) in PBS for 30 min at RT and then incubated with N-specific MAb for 2 h. After being washed five times in PBS, the cells were incubated for 1 h at RT with a goat anti-mouse secondary antibody conjugated to Alexa Fluor 488 (Invitrogen), followed by counterstaining with 4′,6-diamidino-2-phenylindole (DAPI; Sigma-Aldrich). The coverslips were mounted on microscope glass slides in

mounting buffer and cell staining was visualized using a fluorescent Leica DM IL LED microscope (Leica, Wetzlar, Germany). For study of colocalization, MitoTracker Red CMXRos (200 nM; Invitrogen) was added to ST cells under indicated conditions and left for 45 min at 37 °C prior to fixation. The cells were then stained with Bax-, cyt c- or AIF-specific antibody as described above, and cell staining was analyzed using a Confocal Laser Scanning microscope (Carl Zeiss).

2.7. Fluorescence-activated cell sorting (FACS) analysis

Quantification of PDCoV-infected cells upon independent treatment of each reagent was analyzed by flow cytometry. ST cells were pretreated with each inhibitor or DMSO for 1 h, infected with PDCoV, and subsequently maintained in the presence of vehicle or each inhibitor. Virus-infected cells were trypsinized at 24 hpi and centrifuged at 250 × *g* (Hanil Centrifuge FLETA 5, Incheon, South Korea) for 5 min. The cell pellet was washed with cold washing buffer (1% BSA and 0.1% sodium azide in PBS), and 10^6 cells were resuspended in 1% formaldehyde solution in cold wash buffer for fixation at 4 °C in the dark for 30 min followed by centrifugation and incubation of the pellet in 0.2% Triton X-100 in PBS at 37 °C for 15 min for permeabilization. After centrifugation, the cell pellet was resuspended in a solution of the primary anti-N MAb and the mixture was incubated at 4 °C for 30 min. The cells were washed and allowed to react with an Alexa Fluor 488-conjugated anti-mouse IgG secondary antibody at 4 °C for 30 min in the dark. The stained cells were washed again and analyzed on a flow cytometer (BD Biosciences).

2.8. Subcellular fractionation and western blotting

ST cells were grown in 6-well tissue culture plates for 1 day and were mock infected or infected with PDCoV at an MOI of 1. At the indicated times, cells were harvested in 50 μl of lysis

buffer (0.5% TritonX-100, 60 mM β-glycerophosphate, 15 mM ρ-nitro phenyl phosphate, 25 mM MOPS, 15 mM $MgCl_2$, 80 mM NaCl, 15 mM EGTA [pH 7.4], 1 mM sodium orthovanadate, 1 μg/ml E64, 2 μg/ml aprotinin, 1 μg/ml leupeptin, and 1 mM PMSF) and sonicated on ice 5 times for 1 s each. Homogenates were lysed for 30 min on ice, and clarified by centrifugation at 15,800 × *g* (Eppendorf centrifuge 5415R, Hamburg, Germany) for 30 min at 4 °C. For subcellular fractionation, PDCoV-infected ST cells were fractionated using a Nuclear/Cytosol or Mitochondria/Cytosol Fractionation Kit (BioVision, Mountain View, CA) according to the manufacturer's manuals. The total protein concentrations in the supernatants were determined using a BCA protein assay (Pierce, Rockford, IL). Equal amounts of total protein were separated on a NuPAGE 4–12% gradient Bis-Tris gel (Invitrogen) under reducing conditions and electrotransferred onto Immobilon-P (Millipore, Bedford, MA). The membranes were subsequently blocked with 3% powdered skim milk (BD Biosciences) in TBS (10 mM Tris-HCl [pH 8.0], 150 mM NaCl) with 0.05% Tween-20 (TBST) at 4 °C for 2 h and incubated at 4 °C overnight with the primary antibodies. The blots were then incubated with corresponding secondary HRP-labeled antibodies at a dilution of 1:5000 for 2 h at 4 °C. Proteins were visualized using enhanced chemiluminescence (ECL) reagents (GE Healthcare, Piscataway, NJ) according to the manufacturer's instructions. To quantify viral protein production, band densities of each protein were quantitatively analyzed using a computer densitometer with the Wright Cell Imaging Facility (WCIF) version of the ImageJ software package (http://www.uhnresearch.ca/facilities/wcif/imagej/) based on the density value relative to the corresponding housekeeping gene.

2.9. Virus titration

ST cells were PDCoV infected and treated with each chemical or DMSO as described above. The culture supernatant was collected at different time points (6, 9, 12, 18, and 24 hpi) and stored at –80 °C. The PDCoV titer was measured by limiting dilution on ST cells in duplicate as described previously (Jang et al., 2018), and then 50% tissue culture infectious dose ($TCID_{50}$) per ml was calculated using Reed-Muench method (Reed and Muench, 1938).

2.10. Statistical analysis

All statistical analyses were performed using Student's *t* test, and *P*-values of less than 0.05 were considered statistically significant.

3. Results

3.1. PDCoV induces programmed cell death in vitro

To investigate whether the apoptotic cell death was triggered by PDCoV, virus-infected cells were examined for the presence of DNA fragmentation, the hallmark of apoptosis in cells. ST cells were infected with PDCoV and CPE were monitored after infection. Light microscopy of PDCoV-infected ST cells indicated typical CPE characterized by cell rounding, clumping as clusters, and detachment, which were visible starting at 6 hpi and became prominent by 12 hpi (Fig. 1A, upper panels). To detect the intracellular fragmented DNA, cellular DNA from mock- or virus-infected cells was harvested and subjected to a DNA laddering assay. Consistent with the results of CPE observation, intracellular DNA fragmentation appeared at 6 hpi and the DNA ladder pattern was apparent at 9 hpi (Fig. 1A, lower panel). This characteristic of apoptosis was further verified using a TUNEL assay. As shown in Fig. 1B, TUNEL-labeled (DNA damage and dead) cells were only observed within virus-infected cells as compared to mock-infected cells. The

process of PDCoV-induced apoptosis was then assessed by staining the virus- and mock-infected cells with Annexin V/PI followed by FACS analysis to quantitatively determine the percentage of viable, apoptotic, and dead cells. PDCoV infection produced a significant level of apoptosis (Annexin V positive/PI negative) at 6 hpi. The percentage of early-stage apoptotic cells increased with the progression of infection and reached a maximum of 41.6% at 24 hpi (Fig. 1C). In addition, comparable kinetics of apoptosis were observed in ST cells infected with PDCoV at an MOI of 0.1 (data not shown). Taken together, these data confirm that PDCoV infection induced apoptosis *in vitro*.

3.2. Pan-caspase inhibitor treatment inhibits PDCoV-induced apoptosis and impairs PDCoV infection

Caspases are a family of aspartate-specific cysteine protease enzymes that play essential roles during the execution phase of programmed cell death, leading to distinct morphological changes that characterize apoptosis (Clarke and Tyler, 2009). To elucidate the mechanism and type of apoptotic cell death, we initially assessed if a broad-spectrum pan-caspase inhibitor, Z-VAD-FMK, blocks PDCoV-induced apoptosis. The results of the MTT assay revealed that none of the tested Z-VAD-FMK doses caused any change in the cell viability (data not shown). ST cells were treated with Z-VAD-FMK at 100 μM concentration and subjected to viral infection. At the indicated time points post-infection, virus-infected and Z-VAD-FMK-treated cells were analyzed with FACS for the quantification of Annexin V binding. Z-VAD-FMK treatment protected cells from PDCoV-induced apoptosis (Fig. 2A). The percentage of early-phase apoptotic cells was significantly reduced in cells treated with Z-VAD-FMK than in the vehicle (DMSO)-treated cells (second panel) or PDCoV-infected cells during the course of infection (compared to Fig. 1C). The

results of TUNEL assay highlighted the inhibitory effect of Z-VAD-FMK on PDCoV-induced apoptosis, as only few TUNEL-labeled cells were observed in virus-infected cells pretreated with Z-VAD-FMK (data not shown). These results indicate the association of caspases with PDCoV-triggered apoptosis.

We next investigated if the same caspase inhibitor affects PDCoV replication. ST cells were pretreated with Z-VAD-FMK at concentrations of 50 and 100 μM or DMSO (0.5%) for 1 h and then infected with PDCoV. Virus production was determined by monitoring the strength of CPE and confirmed with immunofluorescence at 24 hpi (Fig. 2B). Vehicle-treated control cells showed CPE and were positive for PDCoV N protein-specific staining, indicating infection and spread of the virus to neighboring cells. However, the inhibitory effect of Z-VAD-FMK on viral propagation was clearly detectable. As shown in Fig. 2B, the pan-caspase inhibitor significantly attenuated PDCoV-induced CPE (first panels) and PDCoV gene expression (second panels) in a dose-dependent manner. Quantification of N protein staining results showed that the proportion (%) of virus-infected cells noticeably diminished during Z-VAD-FMK treatment. Z-VAD-FMK inhibited viral replication by nearly 90% at the highest concentration tested (Fig. 2C). Taken together, our data reveal that caspase cascades were activated by PDCoV and their chemical inhibition negatively affected PDCoV-induced apoptotic cell death and viral replication, suggestive of the indispensable role of caspase activation in this process.

3.3. Intrinsic caspase-9 dependent apoptosis pathway is required for PDCoV infection

Apoptosis can be triggered either by an external death receptor stimulus (extrinsic) or through internal (intrinsic) mitochondria-mediated signaling. Although both pathways engage the same proteolytic caspase cascade and interface at the point of downstream executioner caspase-3

activation, initiator caspase-8 and caspase-9 discriminate between the extrinsic and intrinsic pathways, respectively (Clarke and Tyler, 2009). To identify the apoptosis pathway induced by PDCoV, specific inhibitors of caspase-8 or caspase-9 were used. ST cells were pretreated with Z-IETD-FMK (caspase-8 inhibitor) or Z-LEHD-FMK (caspase-9 inhibitor) at concentrations of 50 and 100 μM or DMSO and subjected to virus infection. PDCoV growth measured by CPE observation and IFA was similar between cells treated with Z-IETD-FMK and DMSO (Fig. 3A). In contrast, treatment with Z-LEHD-FMK dramatically weakened PDCoV infectivity in ST cells. The level of PDCoV replication was indirectly measured by the quantification of cells expressing N protein using flow cytometry (Fig. 3B). No impairment in PDCoV propagation was observed in the presence of Z-IETD-FMK, while the treatment of cells with 100 μM Z-LEHD-FMK resulted in ≥80% decrease in PDCoV infection as compared with the control group (DMSO-treated cells). The expression level of PDCoV N protein in the presence of each inhibitor or DMSO was also evaluated with Western blot analysis. Only caspase-9 inhibitor Z-LEHD-FMK exerted a detrimental effect on the viral protein production (Fig. 3C). Densitometric analysis of Western blots revealed that the intracellular expression of N protein was effectively prevented by Z-LEHD-FMK, with an approximately 70% reduction at the highest concentration tested.

Virus yield was determined during treatment with initiator caspase inhibitors to verify the apoptosis pathway involved in PDCoV replication. After infection, viral supernatants were collected at 24 hpi and viral titers were measured. As illustrated in Fig. 4A, only caspase-9 inhibitor suppressed the release of viral progeny in a dose-dependent manner. The peak viral titers in DMSO-treated control and Z-IETD-FMK-treated cells were comparable and ranged between $10^{6.9}$and $10^{7.2}$ $TCID_{50}$/ml. The addition of Z-LEHD-FMK at the highest concentration resulted in the reduction of PDCoV titer to $10^{3.4}$ $TCID_{50}$/ml (almost 4-log reduction as compared to control).

Furthermore, examination of growth kinetics revealed a marked delay in the overall process of PDCoV replication upon treatment of cells with Z-LEHD-FMK (Fig. 4B). These findings demonstrate that the activation of the intrinsic apoptosis pathway is important for the successful replication of PDCoV in ST cells.

To confirm the above results, we determined the activity of initiator and effector caspases during PDCoV infection by Western blot analysis. Caspase-3 is the main executioner caspase activated by both extrinsic and intrinsic apoptotic pathways and causes morphological features of apoptosis. As shown in Fig. 5, a detectable level of cleaved caspase-9 was observed in PDCoV-infected cells by 6 hpi, while its level was obvious at 12 hpi (first panel). Activated effector caspase-3 was similarly detected by 6 hpi and its level was vague yet clearly evident at 12 hpi (second panel). Consistent with kinetics of both initiator and executioner caspase activation, N protein was first detected at 6 hpi, and its production greatly increased thereafter (third panel), indicating the acceleration of caspase cascade activation via the intrinsic apoptotic pathway during the progression of PDCoV replication in ST cells.

3.4. PDCoV infection promotes Bax translocation to the mitochondria and cyt c release to the cytosol

The intrinsic pathway is modulated through the activation of pro-death Bcl-2 family proteins such as Bax, resulting in the formation of Bax-based pores in the mitochondrial outer membrane (MOM). Mitochondrial outer membrane permeabilization (MOMP) leads to the release of cyt c, which sequentially activates initiator caspase-9 and downstream effector caspase-3, thereby orchestrating the final apoptotic response (Clarke and Tyler, 2009). To study the potential role of MOMP in the caspase-dependent pathway of PDCoV-induced apoptosis, we determined

the subcellular localization of Bax and cyt c in PDCoV-infected cells using immunofluorescence confocal microscopy. As shown in Fig. 6A, Bax continued to be localized broadly in the mitochondria after PDCoV infection, evident from its colocalization with a mitochondrial-specific marker. On the other hand, cyt c was present in the cytosolic region and failed to colocalize with the mitochondria marker in the majority of cells infected with PDCoV. These observations were confirmed by Western blot analysis with mitochondrial and cytosolic or nuclear extracts. In comparison with mock-infected cells, PDCoV-infected cells exhibited an independent increase in levels of Bax and cyt c in the mitochondrial and cytosolic extracts, respectively (Fig. 6B, first and second panels). To eliminate the possibility of association between caspase-independent process and PDCoV-triggered apoptosis, we analyzed the translocation of another apoptogenic molecule, apoptosis-inducing factor (AIF), which is proteolytically cleaved and released into the nucleus by MOMP to execute caspase-independent intrinsic apoptosis (Galluzzi et al., 2012). In contrast to cyt c, AIF was detected in the mitochondria but absent in the nucleus throughout PDCoV infection period, as demonstrated from AIF and MitoTracker colocalization and AIF detection in mitochondrial fractions (Fig. 6A and B). AIF retention in the mitochondria during PDCoV infection was concurrent with the execution of caspase-dependent apoptotic cell death by PDCoV as described above. Thus, PDCoV infection triggers Bax recruitment into the mitochondria, leading to MOMP and the consequent release of mitochondrial cyt c to commit cells to death.

3.5. Mitochondrial permeability transition pore (MPTP) inhibition blocks PDCoV-induced apoptosis and PDCoV replication

The present study demonstrates the translocation of the mitochondrial cyt c into the cytoplasm by Bax-mediated MOMP following PDCoV infection. Along with this mechanism, the

mitochondrial permeability transition pore (MPTP) is considered as the most viable model of mitochondrial channels that accounts for MOMP (Suh et al., 2013; Mathupala et al., 2006). Cyclophilin D (CypD) is localized to the mitochondrial membrane matrix and acts as a key component in the process of MPTP opening (Baines et al., 2005; Schinzel et al., 2005). Therefore, we evaluated if CypD inhibition may prevent apoptotic cell death induced by PDCoV. ST cells were treated with cyclosporin A (CsA), a chemical inhibitor of CypD, to prevent MPTP opening upon PDCoV infection. Following CsA treatment, PDCoV-induced apoptosis was quantitatively measured by Annexin V/PI flow cytometry. As shown in Fig. 7A, treatment with CsA notably decreased the percentage of PDCoV-induced early apoptotic cells (second panel) by 7.7 to 11.8% during the course of PDCoV infection (compared to Fig. 2A). DNA laddering assay indicated that Z-VAD-FMK or CsA treatment in PDCoV-infected cells completely abolished the intracellular DNA fragmentation (Fig. 7B, lanes 3 and 4), while cells infected with PDCoV alone clearly displayed a DNA laddering pattern (Fig. 7B, lane 2). These results indicate that CsA-mediated CypD inhibition efficiently suppressed apoptotic cell death executed by PDCoV, suggesting that PDCoV infection may regulate the opening of MPTP.

To assess the effect of CsA on PDCoV propagation, ST cells were pretreated with CsA at concentrations of 5 and 10 μM, and the drug was retained during the infection and subsequent incubation. PDCoV replication was determined by monitoring virus-specific CPE and verified by IFA at 24 hpi (Fig. 8A). In contrast to vehicle-treated control cells, cells treated with CsA showed a strong inhibitory effect on PDCoV propagation, as evident from the dramatic decrease in virus-induced CPE and viral gene expression. The number of cells expressing viral antigen, as quantified by N protein staining, reduced during CsA treatment, with almost 90% inhibition observed at 10 μM concentration (Fig. 8B). We also treated cells with an AIF inhibitor, *N*-phenylmaleimide (*N*-

PhMI), as a negative chemical control that prevents AIF-induced caspase-independent apoptosis (Kim and Lee, 2014; Susin et al., 1996; Wang et al., 2007). Unlike CsA, *N*-PhMI treatment was incapable of inhibiting PDCoV infection even at the highest concentration used (Fig. 8A and B). To further examine the antiviral activity of CsA against PDCoV replication, virus production was determined in the presence or absence of CsA. Western blot analysis revealed that 10 μM CsA treatment significantly prevented the intracellular expression of the viral protein (Fig. 9A). After infection, viral supernatants were collected at 24 hpi and viral titers were measured. As shown in Fig. 9B, CsA treatment significantly reduced the release of viral progeny in a dose-dependent manner. The peak viral titer was determined as $10^{7.5}$ $TCID_{50}$/ml for the vehicle-treated control, whereas the addition of 10 μM CsA declined PDCoV titer to $10^{2.7}$ $TCID_{50}$/ml (almost 5-log reduction as compared with the control). The study of growth kinetics further demonstrated that the overall process of PDCoV replication was severely interfered by CsA (Fig. 9C). Taken together, CsA proficiently suppressed PDCoV replication and inhibited PDCoV-induced apoptosis.

3.6. PDCoV infection causes cyt c release into the cytosol through MPTP opening

As CypD is involved in the alteration of MPTP and subsequent release of proapoptotic factors, it is conceivable that the inhibition of MPTP opening may result in the blocking of cyt c relocation induced by PDCoV, leading to impaired PDCoV-induced apoptosis and viral replication. In this direction, we determined whether CsA specifically affects the cytosolic translocation of cyt c mediated by PDCoV infection. Confocal microscopy results demonstrated that cyt c release in PDCoV-infected cells was distinctly hampered following CsA-mediated inhibition of CypD and cyt c was distributed in the mitochondria during PDCoV infection (Fig. 10A). Mitochondrial retention of cyt c in the presence of CsA was confirmed by a cell fractionation assay. As expected,

the level of cyt c in cytosolic fractions was barely detectable in the presence of CsA, demonstrating that CypD inhibition failed to cause the release of cyt c from the mitochondria into the cytoplasm (Fig. 10B, first panel). Although an increase in Bax level was observed in the mitochondria after 12 hpi (Fig. 10B, lanes 3 and 4 in second panel), CsA treatment reduced mitochondrial Bax (lane 2) and enhanced cytosolic Bax in PDCoV infected cells than in mock-infected cells (lanes 6–8). Altogether, these results indicate that CypD-dependent MPTP activation upon PDCoV infection directly modulated cyt c release, the commitment step in mitochondria-mediated apoptosis, thereby favoring viral replication *in vitro*.

4. Discussion

Apoptosis or programmed cell death is an actively controlled multistep process of cell suicide that occurs in response to a variety of stress conditions, including viral infections. Considering apoptosis as one of the innate immune defense mechanisms, viruses may evade the apoptotic cell death and prolong the survival of infected cells to maximize the production of the viral progeny (Thomson, 2001). However, several viruses promote apoptosis to facilitate the release and dissemination of the viral progeny for further invasion of the neighboring cells. This irreversible death event is characterized with cytolytic features after viral infections, including CPE *in vitro* or/and important biological processes promoting cell damage, tissue injury, and disease severity *in vivo* (Clarke et al., 2009; Clarke and Tyler, 2009; DeDiego et al., 2011; Ding et al., 2013; Doley et al., 2014; Eleouet et al., 1998; Favreau et al., 2012; Kim and Lee, 2014; Lan et al., 2013; Lee and Kleiboeker, 2007; St-Louis and Archambault, 2007; Sarmento et al., 2006; Suzuke et al., 2008; Zhang et al., 2015). The present study demonstrated that PDCoV triggers apoptosis in ST cells, as evident from apoptotic parameters including oligonucleosomal DNA

fragmentation and PS exposure. This finding strongly suggests that the cytopathology of PDCoV infection represented by cell rounding, clumping, and detachment is associated with the apoptotic process that contributes to viral replication.

Both extrinsic and intrinsic apoptotic pathways may activate the corresponding upstream initiator caspases, leading to the processing and activation of downstream common effector caspases to execute apoptosis (Clarke and Tyler, 2009; Galluzzi et al., 2012). To understand the molecular mechanisms underlying apoptosis caused by PDCoV, we focused on the potential involvement of the caspase cascade in the process of apoptosis upon PDCoV infection. Chemical inhibition of caspase activation was shown to prevent PDCoV-induced apoptosis and viral replication. Furthermore, treatment of cells with caspase-9 inhibitor, but not a caspase-8 inhibitor, greatly restricted PDCoV infection, indicative of the involvement of the mitochondria-mediated intrinsic apoptotic pathway in PDCoV infection. The upstream initiator caspase-9 and its downstream effector caspase-3 were proteolytically activated to induce the execution phase of apoptosis. PDCoV infection sequentially activated cleaved (active) forms of caspase-9 and caspase-3 at 6 and 12 hpi, respectively, and their levels increased thereafter with the progression of infection (Fig. 5). Thus, the caspase-dependent apoptotic pathway seems to be manipulated by PDCoV to ensure competent viral replication in target cells.

As a response to various intracellular stimuli, both pro- and anti-apoptotic signals converge toward the mitochondrion-centered control mechanism to provoke intrinsic apoptosis. Under this circumstance, MOMP, an irreversible step leading to apoptosis execution, may be initiated at the outer membrane of the mitochondria through the pore-forming activity of pro-apoptotic Bax subfamily after their mitochondria relocation from the cytoplasm or via an abrupt increase in cell permeability through the opening of MPTP at the inner membrane (Brenner and Grimm, 2006;

Galluzzi et al., 2012; Tait and Green, 2013). This phenomenon permits the release of several apoptosis-mediating molecules, normally retained within the mitochondrial intermembrane space, into the cytosol (Galluzzi et al., 2012). Of these, cytosolic cyt c assembles with other pro-apoptotic factors to form the apoptosome, which triggers the caspase-dependent proteolytic cascade (Galluzzi et al., 2012; Li et al., 1997). On the other hand, AIF, a ubiquitously expressed flavoprotein, critically functions in the caspase-independent apoptosis process by relocating into the nucleus and promoting large-scale DNA fragmentation and cell death (Galluzzi et al., 2012; Joza et al., 2001; Susin et al., 1999). As caspases are relevant to both PDCoV-induced apoptosis and viral replication, we investigated the status of cyt c release from the mitochondria of PDCoV-infected cells. The translocation of Bax into the mitochondria was observed during the early stage of PDCoV infection, wherein it likely participates in the formation of pores in MOM. At the same time, the majority of cyt c was detected and retained thereafter in the cytoplasm of PDCoV-infected cells. On the contrary, the displacement of AIF from the mitochondria to the nucleus was completely absent in PDCoV-infected cells, although porcine epidemic diarrhea virus, another swine enteric coronavirus, is known to relocate mitochondrial AIF to the nucleus to trigger apoptotic cell death (Kim and Lee, 2014). This result further supports the hypothesis that PDCoV triggers apoptosis in a caspase-dependent manner. The association between PDCoV-induced apoptosis and cyt c release and the subsequent caspase activation without AIF nuclear translocation suggest that cyt c is the key pro-apoptotic factor released via alterations in the mitochondrial membrane permeability mediated by Bax proteins and acts directly to execute apoptotic cell death in PDCoV infection.

It is anticipated that apoptosis related to mitochondrial dysfunction may contribute to commitment of PDCoV-infected cells to death. Although we observed continuously lower levels

of cytosolic Bax in PDCoV-infected cells than in mock-infected cells, we were unable to consistently detect increased levels of mitochondrial Bax throughout the entire period of PDCoV infection (Fig. 6B). This observation leads us to speculate that an alternative mechanism with regard to the opening process following MPTP formation may exist to regulate MOMP during PDCoV infection. CsA acts as a specific inhibitor of MPTP opening by inhibiting the activity of CypD that constitutes the MPTP complex in the mitochondrial inner membrane. Our results show that the pharmacological inhibition of MPTP opening with CsA suppressed PDCoV-induced apoptosis, as 80–90% cell survival was observed in CsA-treated cells after PDCoV infection (comparable to mock-infected cells). Furthermore, CsA exerted its antiviral activity through the inhibition of multiple steps of PDCoV life cycle, including viral protein translation and spread of viral progeny. Inhibitory activities of CsA on PDCoV infection were more efficient than those of caspase inhibitors in terms of antiviral effects (5-log versus 3-log reduction) and effective minimal doses (5 μM versus 50 μM), albeit independent treatment with each pan or specific caspase inhibitor also exhibited significant suppression of PDCoV replication in its own way. This discrimination may be attributed to the wide-spectrum antiviral effect of CsA as an inhibitor members of the cellular cyclophilin (Cyp) family via multiple simultaneous mechanisms. In particular, CsA is known to suppress the replication of a variety of RNA viruses, including nidoviruses, by affecting the function of other Cyps, such as CypA and CypB, involved in viral biosynthesis and the interaction with viral constituents (de Wilde et al., 2013; Kambara et al., 2011; Kim and Lee, 2014; Nakagawa et al., 2004; Pfefferle et al., 2011; Qing et al., 2009). Since the present study primarily focused on CypD as an MPTP opening component associated with PDCoV-induced apoptosis, no experiments were conducted to investigate the participation of other Cyps in the replication of PDCoV. However, we cannot exclude that CsA could synchronously

inhibit cellular CypA and CypB that may contribute to PDCoV infection *in vitro*. Although potential roles of these Cyps in PDCoV replication remain to be determined, thus, it is feasible that CsA may synergistically elicit its anti-PDCoV activity through the inhibition of CypD as well as CypA or/and CypB.

The presence of CsA impaired PDCoV-mediated cyt c release into the cytosol, leading to the mitochondrial retention of cyt c. Therefore, CypD-activated MPTP modulation plays a pivotal role in caspase-dependent apoptosis of cells by controlling cyt c release after PDCoV infection. Bax translocation into the mitochondria was also inhibited by CsA at 6 dpi (Fig. 10B) when Bax recruitment into the mitochondria was maximum (Fig. 6B). Bax is displaced toward the mitochondria and may directly interact with CypD to facilitate the formation of MPTP to regulate the cyt c release (Favreau et al., 2012; Kumarswamy and Chandna 2009; Oka et al., 2008). As the transient MPTP opening provides a feedforward signal to augment Bax translocation into the mitochondria, these observations may be consistent with CsA-mediated inhibition of the amplification step.

In summary, our findings reveal that PDCoV induces apoptosis-mediated cell death, a cytolytic mechanism causing CPE *in vitro*. PDCoV-induced apoptosis was accompanied with the activation of caspase cascades and promoted effective viral replication *in vitro*. The mitochondrial translocation of Bax and concomitant cytosolic release of cyt c strongly indicated that Bax-mediated MOMP induces the intrinsic cell death event after PDCoV infection. We demonstrated the essential role of MPTP in apoptosis in response to PDCoV infection. MOMP is the consequence of MPTP opening that results in the collapse of the mitochondrial membrane potential, followed by the characteristic and specific relocalization of cyt c into the cytoplasm to mediate caspase-dependent apoptosis. Furthermore, pharmacological inhibition of MPTP opening

abrogated the life cycle of PDCoV at subcytotoxic doses. Although MOMP necessarily contributes to the execution of PDCoV-induced apoptosis, the upstream intracellular regulatory signal(s) and the viral protein(s) associated with this mitochondrion-centered intrinsic apoptotic pathway mediated by PDCoV are still unclear. Future studies are warranted to identify cellular and viral factors involved in this process. In conclusion, PDCoV infection causes the release of cyt c through MOMP activation mediated by two non-mutually exclusive mechanisms, apoptosis signaling events (Bax translocation and mitochondria permeabilization) and MPTP opening, thereby triggering caspase-dependent apoptotic cell death that is required for PDCoV replication. Our results provide insights into the comprehensive understanding of the relationship between PDCoV and host cells.

Acknowledgments

The authors thank Ji Hyun Jeon for her help in preparing the manuscript. This research was supported by the Basic Science Research Program through the National Research Foundation of Korea (NRF) funded by the Ministry of Education (NRF-2015R1D1A1A09057406).

References

Baines, C.P., Kaiser, R.A., Purcell, N.H., Blair, N.S., Osinska, H., Hambleton, M.A., Brunskill, E.W., Sayen, M.R., Gottlieb, R.A., Dorn, G.W., Robbins, J., Molkentin, J.D., 2005. Loss of cyclophilin D reveals a critical role for mitochondrial permeability transition in cell death. Nature 434, 658–662.

Brenner, C., Grimm, S., 2006. The permeability transition pore complex in cancer cell death. Oncogene 25, 4744–4756.

Chen, Q., Gauger, P., Stafne, M., Thomas, J., Arruda, P., Burrough, E., Madson, D., Brodie, J., Magstadt, D., Derscheid, R., Welch, M., Zhang, J., 2015. Pathogenicity and pathogenesis of a United States porcine deltacoronavirus cell culture isolate in 5-day-old neonatal piglets. Virology 482, 51–59.

Clarke, P., Beckham, J.D., Leser, J.S., Hoyt, C.C., Tyler, K.L., 2009. Fas-mediated apoptotic signaling in the mouse brain following reovirus infection. J. Virol. 83, 6161–6170.

Clarke, P., Tyler, K.L., 2009. Apoptosis in animal models of virus-induced disease. Nat. Rev. Microbiol. 7, 144–155.

DeDiego, M.L., Nieto-Torres, J.L., Jiménez-Guardeño, J.M., Regla-Nava, J.A., Alvarez, E., OliSTs, J.C., Zhao, J., Fett, C., Perlman, S., Enjuanes, L., 2011. Severe acute respiratory syndrome

coronavirus envelope protein regulates cell stress response and apoptosis. PLoS Pathog. 7, e1002315.

de Wilde, A.H., Li, Y., van der Meer, Y., Vuagniaux, G., Lysek, R., Fang, Y., Snijder, E.J., van Hemert, M.J., 2013. Cyclophilin inhibitors block arterivirus replication by interfering with viral RNA synthesis. J. Virol. 87, 1454–1464.

Ding, L., Zhao, X., Huang, Y., Du, Q., Dong, F., Zhang, H., Song, X., Zhang, W., Tong, D., 2013. Regulation of ROS in transmissible gastroenteritis virus-activated apoptotic signaling. Biochem. Biophys. Res. Commun. 442, 33–37.

Doley, J., Singh, L.V., Kumar, G.R., Sahoo, A.P., Saxena, L., Chaturvedi, U., Saxena, S., Kumar, R., Singh, P.K., Rajmani, R.S., Santra, L., Palia, S.K., Tiwari, S., Harish, D.R., Kumar, A., Desai, G.S., Gupta, S., Gupta, S.K., Tiwari, A.K., 2014. Canine parvovirus type 2a (CPV-2a)-induced apoptosis in MDCK involves both extrinsic and intrinsic pathways. Appl. Biochem. Biotechnol. 172, 497–508.

Eleouet, J.F., Chilmonczyk, S., Besnardeau, L., Laude, H., 1998. Transmissible gastroenteritis coronavirus induces programmed cell death in infected cells through a caspase-dependent pathway. J. Virol. 72, 4918–4924.

Favreau, D.J., Meessen-Pinard, M., Desforges, M., Talbot, P.J., 2012. Human coronavirus-induced neuronal programmed cell death is cyclophilin d dependent and potentially caspase dispensable. J. Virol. 86, 81–93.

Galluzzi, L., Kepp, O., Trojel-Hansen, C., Kroemer, G., 2012. Mitochondrial control of cellular life, stress, and death. Circ. Res. 111, 1198–1207.

Hu, H., Jung, K., Vlasova, A.N., Chepngeno, J., Lu, Z., Wang, Q., Saif, L.J., 2015. Isolation and characterization of porcine deltacoronavirus from pigs with diarrhea in the United States. J. Clin. Microbiol. 53, 1537–1548.

Jang, G., Kim, S.H., Lee, Y.J., Kim, S., Lee, D.S., Lee, K.K., Lee. C., 2018. Isolation and characterization of a Korean porcine deltacoronavirus strain KNU16-07. J. Vet. Sci. (in press)

Joza, N., Susin, S.A., Daugas, E., Stanford, W.L., Cho, S.K., Li, C.Y., Sasaki, T., Elia, A.J., Cheng, H.Y., Ravagnan, L., Ferri, K.F., Zamzami, N., Wakeham, A., Hakem, R., Yoshida, H., Kong, Y.Y., Mak, T.W., Zúñiga-Pflücker, J.C., Kroemer, G., Penninger, J.M., 2001. Essential role of the mitochondrial apoptosis-inducing factor in programmed cell death. Nature 410, 549–554.

Jung, K., Hu, H., Eyerly, B., Lu, Z., Chepngeno, J., Saif, L.J., 2015. Pathogenicity of 2 porcine deltacoronavirus strains in gnotobiotic pigs. Emerg. Infect. Dis. 21, 650–654.

Jung, K., Hu, H., Saif, L.J., 2016. Porcine deltacoronavirus induces apoptosis in swine testicular and LLC porcine kidney cell lines in vitro but not in infected intestinal enterocytes *in vivo*. Vet. Microbiol. 182, 57–63.

Kambara, H., Tani, H., Mori, Y., Abe, T., Katoh, H., Fukuhara, T., Taguwa, S., Moriishi, K., Matsuura, Y., 2011. Involvement of cyclophilin B in the replication of Japanese encephalitis virus. Virology 412, 211–219.

Kim, Y., Lee, C., 2014. Porcine epidemic diarrhea virus induces caspase-independent apoptosis through activation of mitochondrial apoptosis-inducing factor. Virology 460-461, 180–193.

Kumarswamy, R., Chandna, S., 2009. Putative partners in Bax mediated cytochrome-c release: ANT, CypD, VDAC or none of them? Mitochondrion 9, 1–8.

Lan, Y., Zhao, K., Wang, G., Dong, B., Zhao, J., Tang, B., Lu, H., Gao, W., Chang, L., Jin, Z., Gao, F., He, W., 2013. Porcine hemagglutinating encephalomyelitis virus induces apoptosis in a porcine kidney cell line via caspase-dependent pathways. Virus Res. 176, 292–297.

Lee, S., Lee, C., 2014. Complete Genome Characterization of Korean Porcine Deltacoronavirus Strain KOR/KNU14-04/2014. Genome Announc. 2, e01191–14.

Lee, S.M., Kleiboeker, S.B., 2007. Porcine reproductive and respiratory syndrome virus induces apoptosis through a mitochondria-mediated pathway. Virology 365, 419–434.

Li, G., Chen, Q., Harmon, K.M., Yoon, K.J., Schwartz, K.J., Hoogland, M.J., Gauger, P.C., Main, R.G., Zhang, J., 2014. Full-Length Genome Sequence of Porcine Deltacoronavirus Strain USA/IA/2014/8734. Genome Announc. 2, e00278–14.

Li, P., Nijhawan, D., Budihardjo, I., Srinivasula, S.M., Ahmad, M., Alnemri, E.S., Wang, X., 1997. Cytochrome c and dATP-dependent formation of Apaf-1/caspase-9 complex initiates an apoptotic protease cascade. Cell 91, 479–489.

Ma, Y., Zhang, Y., Liang, X., Lou, F., Oglesbee, M., Krakowka, S., Li, J., 2015. Origin, evolution, and virulence of porcine deltacoronaviruses in the United States. MBio. 6, e00064.

Madapong, A., Saeng-Chuto, K., Lorsirigool, A., Temeeyasen, G., Srijangwad, A., Tripipat, T., Wegner, M., Nilubol, D., 2016. Complete Genome Sequence of Porcine Deltacoronavirus Isolated in Thailand in 2015. Genome Announc. 4, e00408–16.

Marthaler, D., Raymond, L., Jiang, Y., Collins, J., Rossow, K., Rovira, A., 2014. Rapid detection, complete genome sequencing, and phylogenetic analysis of porcine deltacoronavirus. Emerg. Infect. Dis. 20, 1347–1350.

Mathupala, S.P., Ko, Y.H., Pedersen, P.L., 2006. Hexokinase II: cancer's double-edged sword acting as both facilitator and gatekeeper of malignancy when bound to mitochondria. Oncogene. 25, 4777–4786.

Nakagawa, M., Sakamoto, N., Enomoto, N., Tanabe, Y., Kanazawa, N., Koyama, T., Kurosaki, M., Maekawa, S., Yamashiro, T., Chen, C.H., Itsui, Y., Kakinuma, S., Watanabe, M., 2004. Specific inhibition of hepatitis C virus replication by cyclosporin A. Biochem. Biophys. Res. Commun. 313, 42–47.

Oka, N., Wang, L., Mi, W., Zhu, W., Honjo, O., Caldarone, C.A., 2008. Cyclosporine A prevents apoptosis-related mitochondrial dysfunction after neonatal cardioplegic arrest. J. Thorac. Cardiovasc. Surg. 135, 123–130.

Pfefferle, S., Schöpf, J., Kögl, M., Friedel, C.C., Müller, M.A., Carbajo-Lozoya, J., Stellberger, T., von Dall'Armi, E., Herzog, P., Kallies, S., Niemeyer, D., Ditt, V., Kuri, T., Züst, R., Pumpor, K., Hilgenfeld, R., Schwarz, F., Zimmer, R., Steffen, I., Weber, F., Thiel, V., Herrler, G., Thiel, H.J., Schwegmann-Wessels, C., Pöhlmann, S., Haas, J., Drosten, C., von Brunn, A., 2011. The SARS-coronavirus-host interactome: identification of cyclophilins as target for pan-coronavirus inhibitors. PLoS Pathog. 7, e1002331.

Qing, M., Yang, F., Zhang, B., Zou, G., Robida, J.M., Yuan, Z., Tang, H., Shi, P.Y., 2009. Cyclosporine inhibits flavivirus replication through blocking the interaction between host cyclophilins and viral NS5 protein. Antimicrob. Agents Chemother. 53, 3226–3235.

Reed, L.J., Muench, H., 1938. A Simple Method of Estimating Fifty Percent Endpoints. Am. J. Epidemiol. 27, 493–497.

Saeng-Chuto, K., Stott, C.J., Wegner, M., Senasuthum, R., Tantituvanont, A., Nilubol, D., 2017. Retrospective investigation and evolutionary analysis of a novel porcine deltacoronavirus strain detected in Thailand from 2008 to 2015. Arch. Virol. 162, 2103–2108.

Sarmento, L., Tseggai, T., Dhingra, V., Fu, Z.F., 2006. Rabies virus-induced apoptosis involves caspase-dependent and caspase-independent pathways. Virus Res. 121, 144–151.

Schinzel, A.C., Takeuchi, O., Huang, Z., Fisher, J.K., Zhou, Z., Rubens, J., Hetz, C., Danial, N.N., Moskowitz, M.A., Korsmeyer, S.J., 2005. Cyclophilin D is a component of mitochondrial permeability transition and mediates neuronal cell death after focal cerebral ischemia. Proc. Natl. Acad. Sci. USA 102, 12005–12010.

Song, D., Zhou, X., Peng, Q., Chen, Y., Zhang, F., Huang, T., Zhang, T., Li, A., Huang, D., Wu, Q., He, H., Tang, Y., 2015. Newly Emerged Porcine Deltacoronavirus Associated With Diarrhoea in Swine in China: Identification, Prevalence and Full-Length Genome Sequence Analysis. Transbound. Emerg. Dis. 62, 575–580.

St-Louis, M.C., Archambault, D., 2007. The equine arteritis virus induces apoptosis via caspase-8 and mitochondria-dependent caspase-9 activation. Virology 367, 147–155.

Suh, D.H., Kim, M.K., Kim, H.S., Chung, H.H., Song, Y.S., 2013. Mitochondrial permeability transition pore as a selective target for anti-cancer therapy. Front. Oncol. 3, 41.

Susin, S.A., Lorenzo, H.K., Zamzami, N., Marzo, I., Snow, B.E., Brothers, G.M., Mangion, J., Jacotot, E., Costantini, P., Loeffler, M., Larochette, N., Goodlett, D.R., Aebersold, R., Siderovski, D.P., Penninger, J.M., Kroemer, G., 1999. Molecular characterization of mitochondrial apoptosis-inducing factor. Nature 397, 441–446.

Susin, S.A., Zamzami, N., Castedo, M., Hirsch, T., Marchetti, P., Macho, A., Daugas, E., Geuskens, M., Kroemer, G., 1996. Bcl-2 inhibits the mitochondrial release of an apoptogenic protease. J. Exp. Med. 184, 1331–1341.

Suzuki, K., Matsui, Y., Miura, Y., Sentsui, H., 2008. Equine coronavirus induces apoptosis in cultured cells. Vet. Microbiol. 129, 390–395.

Tait, S.W., Green, D.R., 2013. Mitochondrial regulation of cell death. Cold Spring Harb. Perspect. Biol. 5, a008706.

Thomson, B.J., 2001. Viruses and apoptosis. Int. J. Exp. Pathol. 82, 65–76.

Wang, M.J., Liu, S., Liu, Y., Zheng, D., 2007. Actinomycin D enhances TRAIL-induced caspase-dependent and -independent apoptosis in SH-SY5Y neuroblastoma cells. Neurosci. Res. 59, 40–46.

Wang, Y.W., Yue, H., Fang, W., Huang, Y.W., 2015. Complete Genome Sequence of Porcine Deltacoronavirus Strain CH/Sichuan/S27/2012 from Mainland China. Genome Announc. 3, e00945–15.

Woo, P.C., Lau, S.K., Tsang, C.C., Lau, C.C., Wong, P.C., Chow, F.W., Fong, J.Y., Yuen, K.Y., 2012. Coronavirus HKU15 in respiratory tract of pigs and first discovery of coronavirus quasispecies in 5'-untranslated region. Emerg. Microbes Infect. 6, e53.

Zhang, H., Huang, Y., Du, Q., Luo, X., Zhang, L., Zhao, X., Tong, D., 2015. Porcine parvovirus infection induces apoptosis in PK-15 cells through activation of p53 and mitochondria-mediated pathway. Biochem. Biophys. Res. Commun. 456, 649–655.

Figure captions

Fig. 1. PDCoV infection induces apoptosis *in vitro*. (A) CPE and DNA fragmentation in PDCoV-infected cells. ST cells were mock-infected or infected with PDCoV. At the indicated time points after infection, PDCoV-specific CPE were photographed using an inverted microscope at a magnification of 200× (top panels). For DNA fragmentation assay, DNA was extracted from mock- or PDCoV-infected cells and nucleosomal DNA fragmentation of cells was analyzed by agarose gel electrophoresis (bottom panel). As a positive control (PC), cells were treated with staurosporine for 24 h to induce apoptosis. Lane M represents a 1-kb ladder as a DNA molecular-weight size marker. (B) TUNEL labeling of PDCoV-infected cells. Mock-infected control and PDCoV-infected cells fixed at 24 hpi were labeled with TUNEL (green) and sequentially stained with an anti-PDCoV-N antibody (red). Cells were counterstained with DAPI, and photomicrographs of TUNEL labeling and N protein staining in virus-infected cells were obtained using a confocal microscope at 400× magnification. In a merged image, all TUNEL-positive cells were localized within the nuclei of the corresponding PDCoV-infected cells. (C) Cell death analysis by flow cytometry with dual Annexin V-PI cell labeling. PDCoV-infected cells collected at different time points were subjected to dual Annexin V and PI labeling and analyzed by FACS. Lower left quadrants represent intact cells (Annexin V negative/PI negative); Lower right quadrants represent early apoptotic cells (Annexin V positive/PI negative); Upper right quadrants indicate late apoptotic and/or necrotic cells (Annexin V positive/PI negative); and Upper left quadrants indicate necrotic cells (Annexin V negative/PI positive). The figure is representative of three independent experiments. The graph on the right represents the percentage of each quadrant and the non-significant percentages of Annexin V-positive and PI-negative cells were excluded.

Fig. 2. Pan-caspase inhibitor affects PDCoV-induced apoptosis and PDCoV infection. (A) FACS with dual Annexin V-PI cell labeling in the presence of Z-VAD-FMK. ST cells were pretreated with DMSO (0.5%; vehicle control) or Z-VAD-FMK (100 μM) for 1 h, followed by their mock or PDCoV infection. Cells were harvested at the indicated time points, dually labeled with Annexin V and PI, and subjected to FACS analysis. The right graph represents the percentage of each quadrant. (B) PDCoV replication in the presence of Z-VAD-FMK. ST cells were treated with Z-VAD-FMK at the indicated concentrations for 1 h prior to infection with PDCoV. PDCoV-infected cells were maintained for 24 h in the presence of vehicle or Z-VAD-FMK. PDCoV-specific CPE was observed daily and photographed at 24 hpi using an inverted microscope at a magnification of 200× (first panels). For immunostaining, infected cells were fixed at 12 hpi and incubated with MAb against PDCoV N protein, followed by incubation with Alexa green-conjugated goat anti-mouse secondary antibody (second panels). The cells were counterstained with DAPI (third panels) and examined using a fluorescent microscope at 200× magnification. (C) PDCoV production in the presence of Z-VAD-FMK was calculated by measuring the percentage of cells expressing N proteins through flow cytometry. The values shown are the representative of the means from three independent experiments and the error bars represent standard deviations. *, $P < 0.05$; **, $P < 0.001$.

Fig. 3. Treatment with caspase-9 inhibitor but not caspase-8 inhibitor attenuates PDCoV infection. (A) PDCoV propagation in the presence of Z-IETD-FMK (caspase-8 inhibitor) or Z-LEHD-FMK (caspase-9 inhibitor). ST cells were pretreated with each inhibitor at the indicated concentrations for 1 h and then infected with PDCoV. PDCoV-infected cells were further maintained for 24 h in the presence of vehicle, Z-IETD-FMK, or Z-LEHD-FMK. PDCoV-specific CPE were observed

daily and photographed at 24 hpi using an inverted microscope at a magnification of 200× (first panels). At 12 hpi, virus-infected cells were subjected to IFA with an anti-PDCoV N antibody (second panels), followed by DAPI counterstaining (third panels) and examination under a fluorescent microscope at 200× magnification. (B) PDCoV production in the presence of each inhibitor was calculated by measuring the percentage of cells expressing N proteins through flow cytometry. (C) Viral protein translation in the presence of Z-IETD-FMK or Z-LEHD-FMK. Inhibitor-treated ST cells were mock-infected or infected with PDCoV for 1 h and cultivated in the presence or absence of each inhibitor. At 24 hpi, cellular lysates were examined by western blotting with an antibody against PDCoV N protein. The blot was also reacted with a mouse MAb against β-actin to verify equal protein loading. Each viral protein expression was quantitatively analyzed by densitometry in terms of the density value relative to that of β-actin. Inhibitor-treated samples were compared to DMSO-treated control. The values shown are the representative of the means from three independent experiments and the error bars denote standard deviations. *, $P < 0.05$; **, $P < 0.001$.

Fig. 4. Chemical inhibition of caspase-9 activation reduces viral progeny production. (A) ST cells were pretreated with DMSO, Z-IETD-FMK, or Z-LEHD-FMK for 1 h and were mock or PDCoV infected. Vehicle or each inhibitor was present in the medium throughout the infection. At 24 hpi, viral supernatants were collected and viral titers were determined. (B) Growth kinetics of PDCoV upon treatment with each inhibitor was assessed as mentioned in panel A. At the indicated time points after infection, culture supernatants were harvested and virus titers were measured. The results are expressed as the mean values from triplicate wells and the error bars represent standard deviations. *, $P < 0.05$; **, $P < 0.001$.

Fig. 5. PDCoV infection activates the upstream initiator caspase-9 and downstream effector caspase-3. The cellular lysates were collected at the indicated times post-infection, and examined by western blotting using an antibody against caspase-9 (top panel), caspase-3 (second panel), or PDCoV N protein (third panel). The blot was also reacted with a mouse MAb against β-actin to verify equal protein loading (bottom panel). Figures are the representative of the results of three independent experiments.

Fig. 6. PDCoV infection promotes Bax translocation and cyt c release but not AIF translocation. (A) Immunofluorescent detection of Bax, cyt c, and AIF. At 12 hpi, mock-infected or PDCoV-infected ST cells were labeled with MitoTracker Red CMXRos (red), fixed, and independently incubated with a primary antibody against Bax, cyt c, or AIF (green). Bax mitochondrial translocation is represented as the merger of Bax and mitochondrial marker (yellow), while the residual cytosolic localization is indicated by single staining signal (green). Conversely, cyt c cytosolic translocation is represented by single staining signal (green), and residual mitochondrial accumulation is indicated as the merger of cyt c and MitoTracker (yellow). AIF mitochondrial retention is represented as the merger of AIF and mitochondrial marker (yellow). The inset images are enlarged versions of parts of the picture. (B) Western blot analysis for Bax, cyt c, and AIF. The mitochondrial, cytosolic, and nuclear fractions were subjected to western blotting with an antibody directed against Bax (top panel), cyt c (second panel), VDAC (mitochondrial protein marker; third panel), α-tubulin (cytosolic protein marker; fourth panel), AIF (fifth panel), or Sp1 (nuclear protein marker; bottom panel). Lane M, mock-infected samples. All subcellular protein markers served as loading controls. The number under each band represents the fold change in each apoptosis-related

protein level expressed as the densitometric unit of the band normalized to the corresponding loading control level as compared to the mock-infected control. The values shown are the representative of the means from three independent experiments.

Fig. 7. CsA treatment diminishes PDCoV-induced apoptosis. (A) FACS with dual Annexin V-PI cell labeling in the presence of CsA. ST cells were pretreated with DMSO or CsA (10 μM) for 1 h and mock-infected or infected with PDCoV in the presence of vehicle or CsA. Cells were harvested at the indicated time points, dually labeled with Annexin V and PI, and subjected to FACS analysis. The bottom graph represents the percentage of each quadrant. (B) DNA fragmentation analysis in the presence of CsA. ST cells were preincubated with Z-VAD-FMK (100 μM) or CsA (10 μM) for 1 h and infected with mock virus or PDCoV. Nucleosomal DNA fragmentation of the cells was analyzed by agarose gel electrophoresis. Lane M, DNA molecular-weight marker; lane 1, mock-infected and non-treated; lane 2, only PDCoV-infected; lane 3, PDCoV-infected and Z-VAD-FMK-treated; lane 4, PDCoV-infected and CsA-treated.

Fig. 8. CsA treatment suppresses PDCoV propagation. (A) PDCoV infection in the presence of CsA. ST cells were treated with DMSO, CsA, or *N*-PhMI (negative chemical control) at the indicated concentrations for 1 h prior to their infection with PDCoV. PDCoV-infected cells were further maintained for 48 h in the presence of vehicle or CsA. PDCoV-specific CPE was observed daily and photographed at 24 hpi using an inverted microscope at a magnification of 200× (first panels). For immunostaining, infected cells were fixed at 12 hpi and stained with an anti-PDCoV N protein antibody, followed by incubation with Alexa green-conjugated goat anti-mouse secondary antibody (second panels). The cells were counterstained with DAPI (third panels) and

examined using a fluorescent microscope at 200× magnification. (B) Virus production in the presence of CsA or *N*-PhMI was calculated by measuring the percentage of cells expressing N proteins with flow cytometry. The values shown are the representative of the means of three independent experiments and error bars represent standard deviations. **, $P < 0.001$.

Fig. 9. CsA impairs viral protein translation and viral progeny production. (A) Viral protein biosynthesis in the presence of CsA. CsA-treated ST cells were mock-infected or infected with PDCoV for 1 h and cultivated in the presence or absence of CsA. At 24 hpi, cellular lysates were examined by western blotting using an antibody against PDCoV N protein. The blot was also reacted with an anti-β-actin antibody to verify equal protein loading. PDCoV N protein expression was quantitatively analyzed by densitometry by normalizing the density value to that of β-actin and CsA-treated sample results were compared to DMSO-treated control results. The values shown are the representative of the means from three independent experiments and the error bars denote standard deviations. **, $P < 0.001$. (B) Release of viral progeny in the presence of CsA. ST cells were pretreated with DMSO or CsA for 1 h and were mock- or PDCoV-infected. At 24 hpi, virus supernatants were collected and viral titers were determined. The results are expressed as the mean values from triplicate wells, and the error bars represent standard deviations. **, $P < 0.001$. (C) Growth kinetics of PDCoV upon CsA treatment. At the indicated time points after infection, culture supernatants were harvested and viral titers were measured.

Fig. 10. CsA treatment blocks the release of the mitochondrial cyt c. (A) Immunofluorescent detection of cyt c and Bax in the presence of CsA. ST cells were preincubated with CsA (10 μM) for 1 h and were mock-infected or infected with PDCoV. At 12 hpi, cells were labeled with

MitoTracker Red CMXRos (red), fixed, and incubated with a primary antibody against cyt c or Bax (green). Cyt c mitochondrial colocalization is represented as the merger of cyt c and mitochondrial marker (yellow). (B) Western blot analysis of cyt c and Bax in the presence of CsA. Each mitochondrial and cytosolic fraction was prepared under indicated conditions and subjected to western blotting with an antibody against cyt c (top panel), Bax (second panel), VDAC (mitochondrial protein marker; third panel), or α-tubulin (cytosolic protein marker; bottom panel). Lane M, mock-infected. The number under each band represents the fold change in each apoptosis-related protein level expressed as the densitometric unit of the band normalized to the corresponding loading control level as compared to the mock-infected control. The values shown are the representative of the means from three independent experiments.

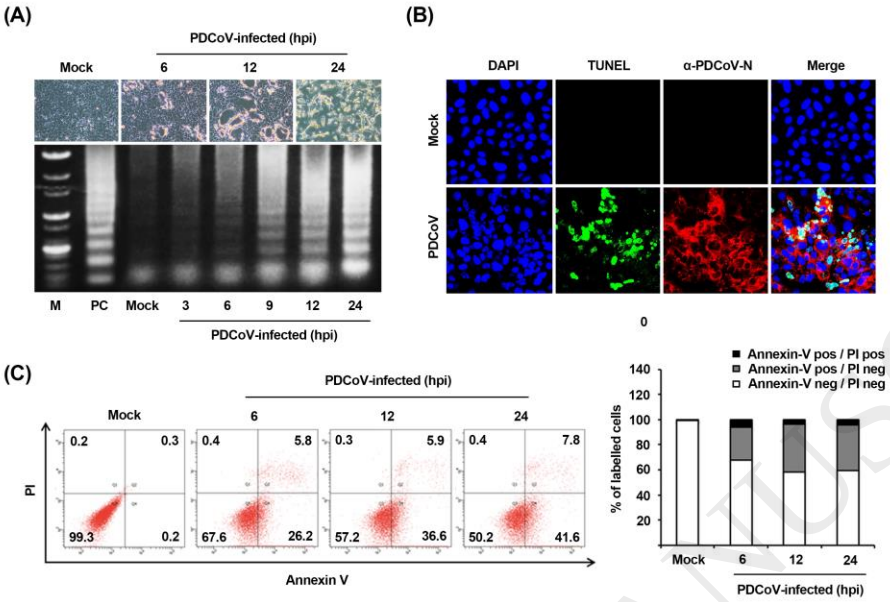

Fig. 1

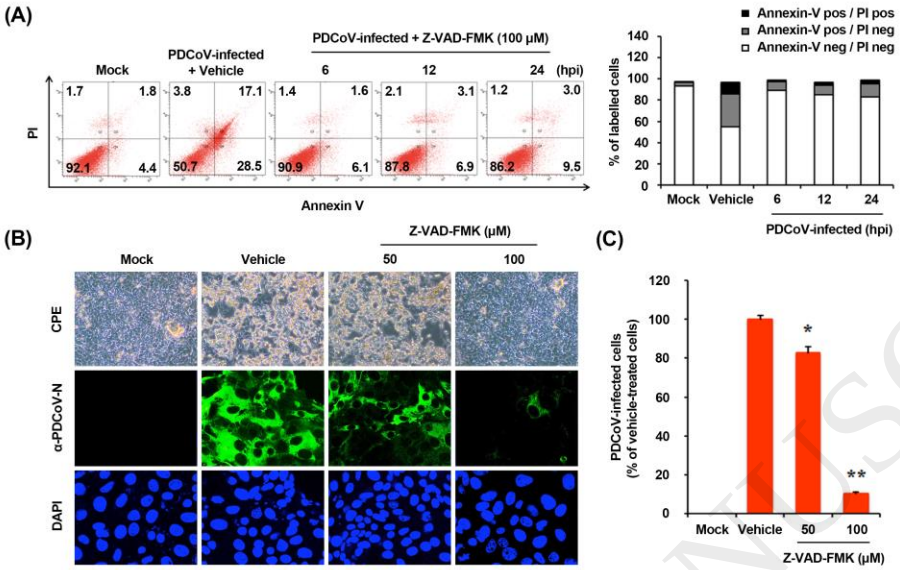

Fig. 2

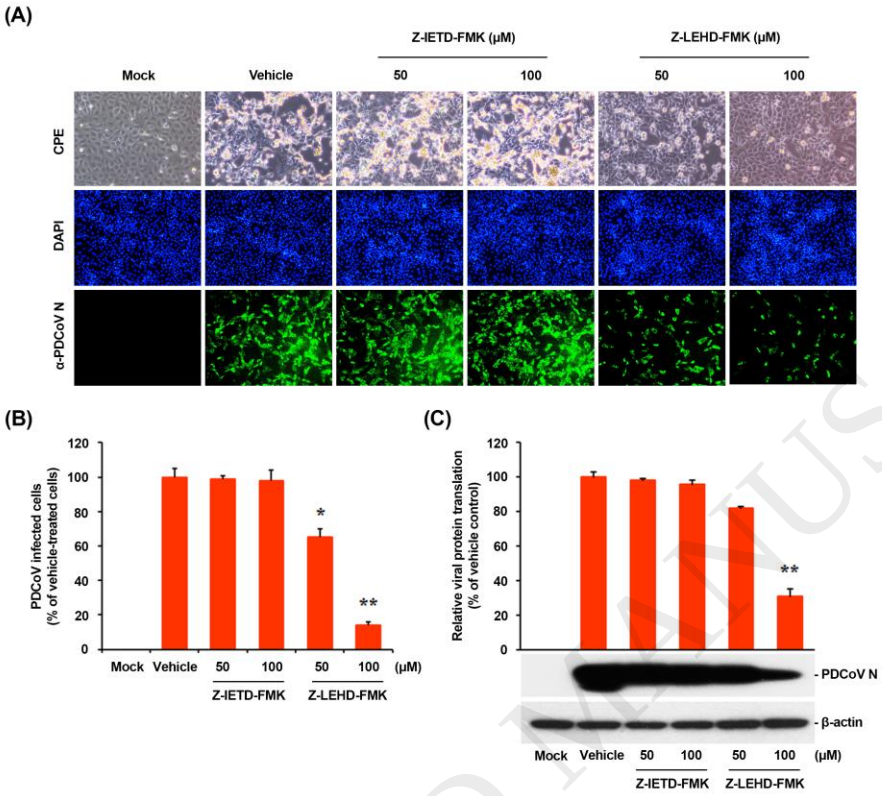

Fig. 3

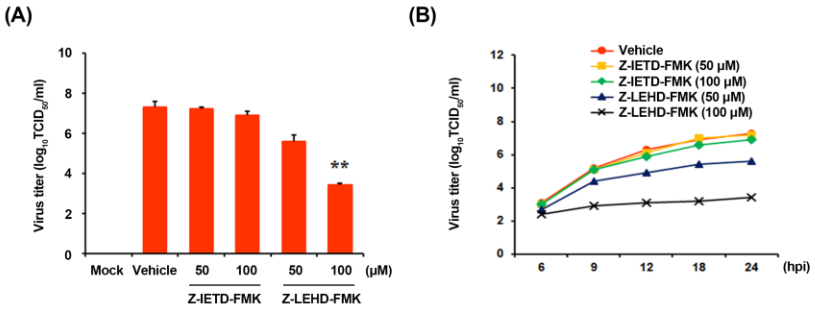

Fig. 4

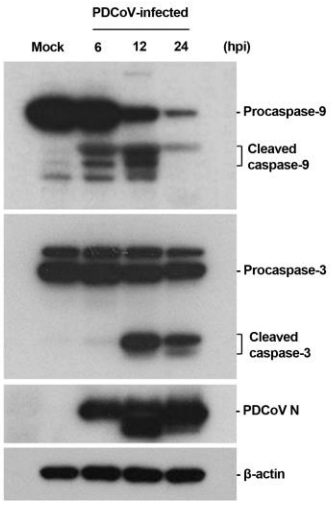

Fig. 5

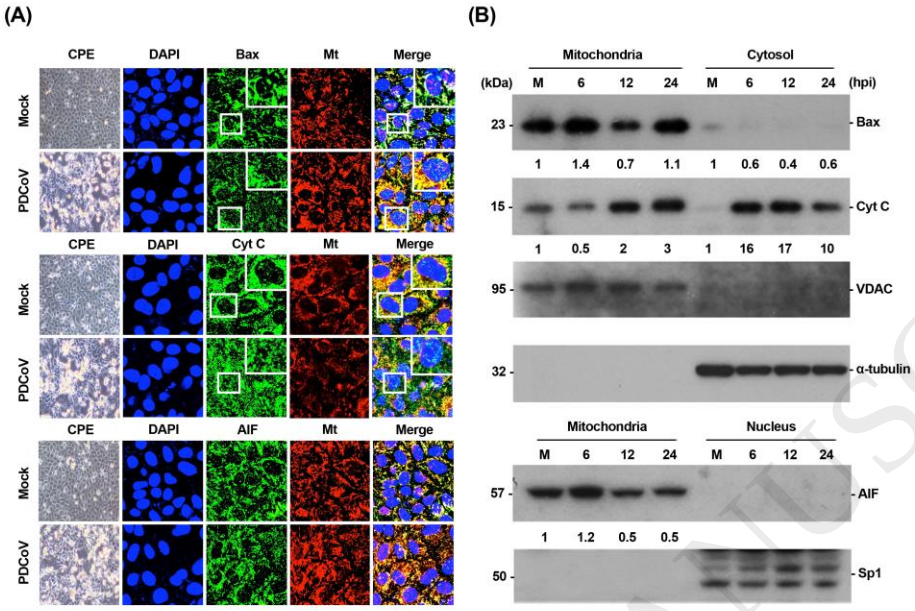

Fig. 6

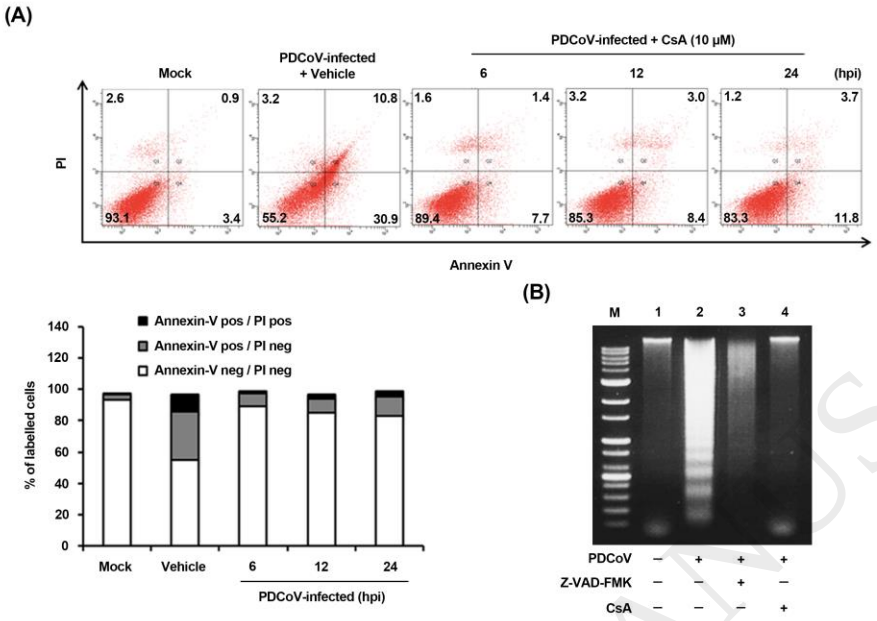

Fig. 7

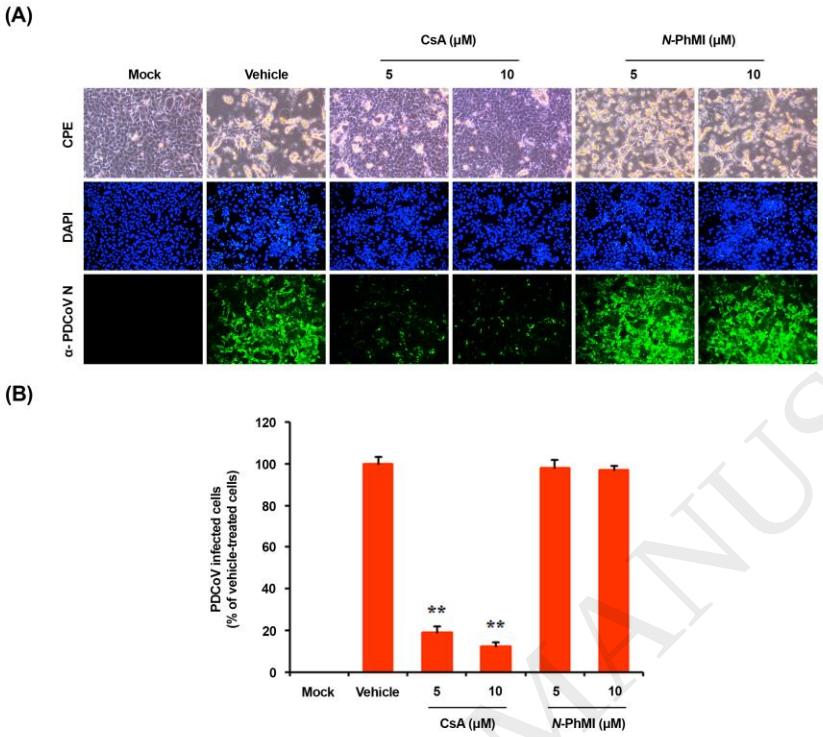

Fig. 8

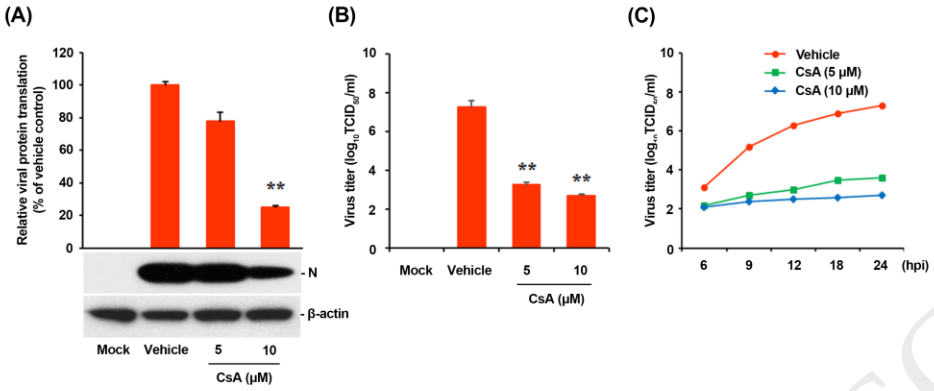

Fig. 9

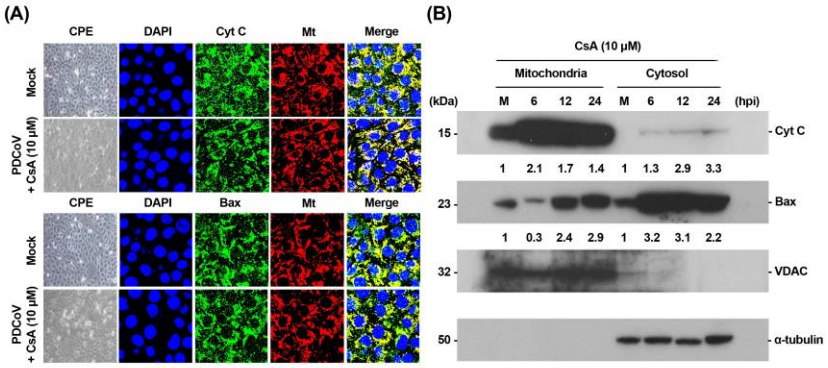

Fig. 10